

Multiple Magnetic Bilayers and Unconventional Criticality without Frustration in $\text{BaCuSi}_2\text{O}_6$

S. Allenspach,^{1,2} A. Biffin,³ U. Stuhr,³ G. S. Tucker,^{3,4} S. Ohira-Kawamura,⁵ M. Kofu,⁵ D. J. Voneshen,⁶ M. Boehm,⁷ B. Normand,¹ N. Laforencie,⁸ F. Mila,⁴ and Ch. Rüegg^{1,2}

¹*Neutrons and Muons Research Division, Paul Scherrer Institut, CH-5232 Villigen, Switzerland*

²*Department of Quantum Matter Physics, University of Geneva, CH-1211 Geneva, Switzerland*

³*Laboratory for Neutron Scattering and Imaging,*

Paul Scherrer Institut, CH-5232 Villigen, Switzerland

⁴*Institute of Physics, École Polytechnique Fédérale de Lausanne (EPFL), CH-1015 Lausanne, Switzerland*

⁵*J-PARC Center, Japan Atomic Energy Agency, Tokai, Ibaraki 319-1195, Japan*

⁶*ISIS Facility, Rutherford Appleton Laboratory, Chilton, Didcot OX11 0QX, United Kingdom*

⁷*Institut Laue Langevin, 6 Rue Jules Horowitz BP156, 38024 Grenoble Cedex 9, France*

⁸*Laboratoire de Physique Théorique, CNRS and Université de Toulouse, 31062 Toulouse, France*

The dimerized quantum magnet $\text{BaCuSi}_2\text{O}_6$ was proposed as an example of “dimensional reduction” arising near the magnetic-field-induced quantum critical point (QCP) due to perfect geometrical frustration of its inter-bilayer interactions. We demonstrate by high-resolution neutron spectroscopy experiments that the effective intra-bilayer interactions are ferromagnetic, thereby excluding frustration. We explain the apparent dimensional reduction by establishing the presence of three magnetically inequivalent bilayers, with ratios 3:2:1, whose differing interaction parameters create an extra field-temperature scaling regime near the QCP with a non-trivial but non-universal exponent. We demonstrate by detailed quantum Monte Carlo simulations that the magnetic interaction parameters we deduce can account for all the measured properties of $\text{BaCuSi}_2\text{O}_6$, opening the way to a quantitative understanding of non-universal scaling in any modulated layered system.

A foundation stone of statistical physics is the theory of classical and quantum criticality [1, 2], which states that all physical properties around a quantum phase transition (QPT) obey universal scaling laws dependent only on the dimension of space, d , and the dynamical exponent, z (the “dimension of time” arising from the dispersion $\omega \propto k^z$ of low-energy excitations). The idea that perfectly frustrated competing interactions could lead to an effective reduction of d has been both proposed [3–5] and contested [6–8] to explain the physics of $\text{BaCuSi}_2\text{O}_6$. This $S = 1/2$ material, known as Han purple from its use as a pigment in ancient China [9, 10], presents a three-dimensional (3D) stack of Cu^{2+} bilayers [Fig. 1(a)] with dominant antiferromagnetic (AF) dimerization, significant intra-bilayer interactions, and a geometrically exact offset between adjacent bilayers, but was reported to show 2D scaling exponents around the field-induced QPT [3]. The discovery of inequivalent bilayers in $\text{BaCuSi}_2\text{O}_6$ [11, 12] raised the question of whether frustration or structural modulation, or both, would be required to explain the apparent dimensional reduction [3]; despite intensive investigation [4, 5, 7, 8, 12–16], this issue has yet to be resolved, with far-reaching implications for any layered material.

While field-driven QPTs from the “quantum disordered” dimerized state to the field-induced ordered state have remained a hot topic in quantum magnetism for multiple reasons (“Bose-Einstein condensation of magnons”) [17], several recent developments make this the right time to revisit dimensional reduction in $\text{BaCuSi}_2\text{O}_6$. First, an *ab initio* analysis of the magnetic

interactions has suggested that the effective intra-bilayer interactions are ferromagnetic (FM) [18], which would preclude a frustration scenario. Second, a systematic structural determination [16] has confirmed at minimum two inequivalent and alternating bilayer units. Third, a new generation of time-of-flight (TOF) neutron spectrometers now allows magnetic excitations in materials such as $\text{BaCuSi}_2\text{O}_6$ to be characterized with unprecedentedly high resolution, and across multiple Brillouin zones.

In this Letter, we report the results of neutron spectroscopy experiments performed to determine the full magnetic Hamiltonian of $\text{BaCuSi}_2\text{O}_6$. We verify that the effective intra-bilayer interaction parameter is FM, establish the presence of three inequivalent bilayers with number ratios 3:2:1, and determine the very weak inter-bilayer interaction. We demonstrate by quantum Monte Carlo (QMC) simulations that our deduced interactions are completely consistent with all prior experimental data for the magnetization, phase diagram, layer triplet populations, and quantum critical behavior. Our conclusion that structural modulation creates an additional regime of unconventional effective scaling behavior will have broad applicability in the age of designer assembly of atomically thin magnetic materials.

The room-temperature crystal structure of $\text{BaCuSi}_2\text{O}_6$ is tetragonal, but becomes weakly orthorhombic below 90 K [19–21]. As Fig. 1(a) represents, the stacked “bilayers”, square lattices of Cu^{2+} spin dimers, have a relative shift of $(\frac{1}{2} \frac{1}{2})$ in the ab plane [in the minimal unit cell of one bilayer [9, 22], represented in Fig. 1(b)]. The

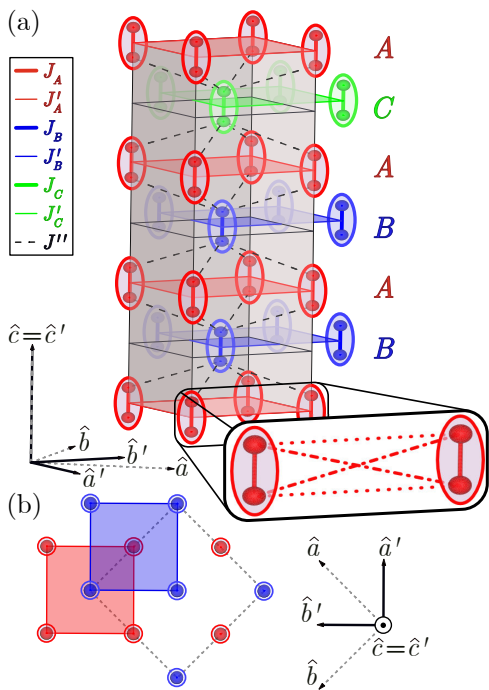


FIG. 1. (a) Schematic representation of one unit cell of the minimal magnetic model for $\text{BaCuSi}_2\text{O}_6$; $\{J_\sigma, J'_\sigma, J''\}$ are Heisenberg interactions. The three distinct bilayer types are labeled A , B , and C . The effective interdimer interaction parameters within each bilayer (J'_σ , edges of colored squares) result from four pairwise ionic interactions (inset). (b) Top view of the ab plane. The minimal unit cell, containing one dimer per bilayer [9, 22], has basis vectors $\{\hat{a}', \hat{b}', \hat{c}'\}$; the crystallographic unit cell, used in previous scattering studies [11, 16, 19], has basis $\{\hat{a}, \hat{b}, \hat{c}\}$ and contains two.

orthorhombic phase contains at least two structurally distinct bilayer types [16, 19], presumably with different intra-bilayer interaction parameters, and with a very weak supercell structure showing incommensurate peaks [12] near $Q_k = 1/8$ [19]. Using the crystallographic unit cell [16, 19] [Fig. 1(b)] to interpret the measured dispersion relations [11] creates an ambiguity between FM and AF intra-bilayer interactions, as detailed in Sec. S1 of the Supplemental Material (SM) [23], which we resolve by working in the minimal unit cell. From the experimental map of the dynamical structure factor that we obtain over multiple Brillouin zones, we demonstrate that the minimal magnetic model is that shown in Fig. 1(a) and deduce the values of all the interaction parameters.

We have performed high-resolution inelastic neutron scattering (INS) measurements on the direct-geometry TOF spectrometers AMATERAS at the J-PARC neutron source [37] and LET at ISIS [38]. Respective measurement temperatures were 0.3 and 1.6 K. On both instruments, incident neutrons of energy $E_i = 9$ meV observe the full band width of the magnetic excitations (3–6 meV at zero applied field). The triple-axis spectrometers

TASP and EIGER at the SINQ neutron source [39] were used for further investigation of selected \vec{Q} directions, measuring at 1.6 K on both. All experiments used one $\text{BaCuSi}_2\text{O}_6$ single crystal, of weight 1.01 g, which we discuss in Sec. S2 of the SM [23].

TOF intensity data for four high-symmetry directions in \vec{Q} space are shown as functions of energy transfer in Figs. 2(a)-2(d). Figures 3(a) and 3(b) show the measured mode energies and Figs. 3(c) and 3(d) their intensities, both obtained using Gaussian fits for selected \vec{Q} points. The EIGER data integrate over a broad energy range to obtain high-statistics information for the combined mode intensities over an extended $|\vec{Q}|$ range. Details of data pre-processing and the Gaussian fitting procedure are presented in Sec. S3 of the SM [23].

Our results show clearly the presence of three distinct excitations in large regions of the Brillouin zone [Figs. 2(a), 2(b), 2(d), and 3(a)]. These must result from three different types of bilayer, and so we label them A , B , and C in ascending order of energy. This confirms the result of Ref. [11], but over a much wider $|\vec{Q}|$ range. Where only two modes are visible because B and C are close in energy [Figs. 2(c) and 3(b)], we label the effective composite mode $B+C$.

We draw attention to three qualitative features of our data, which all lie beyond the results of Ref. [11]. (i) The minima of the strongly dispersive modes in Figs. 2(a), 2(b), and 3(a) give an unambiguous statement about the sign of the intra-bilayer interactions when working in the minimal unit cell. (ii) Although the inter-bilayer interaction is very weak, making the bands in Fig. 2(c) almost flat, it can be determined from the variation of the intensity with Q_l . (iii) Where this band dispersion becomes Q_l independent, in Fig. 2(d), the data can be used to establish the relative intensities of the three separate bilayer contributions.

The magnetic excitations of the dimerized $S = 1/2$ system are “triplon” quasiparticles. To model the triplon spectrum in $\text{BaCuSi}_2\text{O}_6$, we generalized the method of Refs. [40, 41] as outlined in Sec. S4 of the SM [23]. We assume that the only magnetic interactions are those of Fig. 1(a) and, given the weak anisotropies measured in $\text{BaCuSi}_2\text{O}_6$ [42], that they have purely Heisenberg character. A quantitative fit of the complete mode energy and intensity data yields the intradimer interaction parameters $J_A = 4.275(5)$, $J_B = 4.72(1)$, and $J_C = 4.95(2)$ meV, intra-bilayer interactions $J'_A = -0.480(3)$, $J'_B = -0.497(8)$, and $J'_C = -0.57(1)$ meV, and the inter-bilayer interaction $J'' = -0.04(1)$ meV, where $J > 0$ refers to AF interactions and $J < 0$ to FM. The quoted errors are statistical. These optimal values were used to calculate the spectra shown in Figs. 2(e)-2(h) and as the lines in Fig. 3. As part of the fitting process, we used the high- $|\vec{Q}|$ EIGER data to deduce the anisotropic magnetic form factor (Sec. S5 of the SM [23]), which confirms the concentration of spin density within the bilayers [18, 42]. We

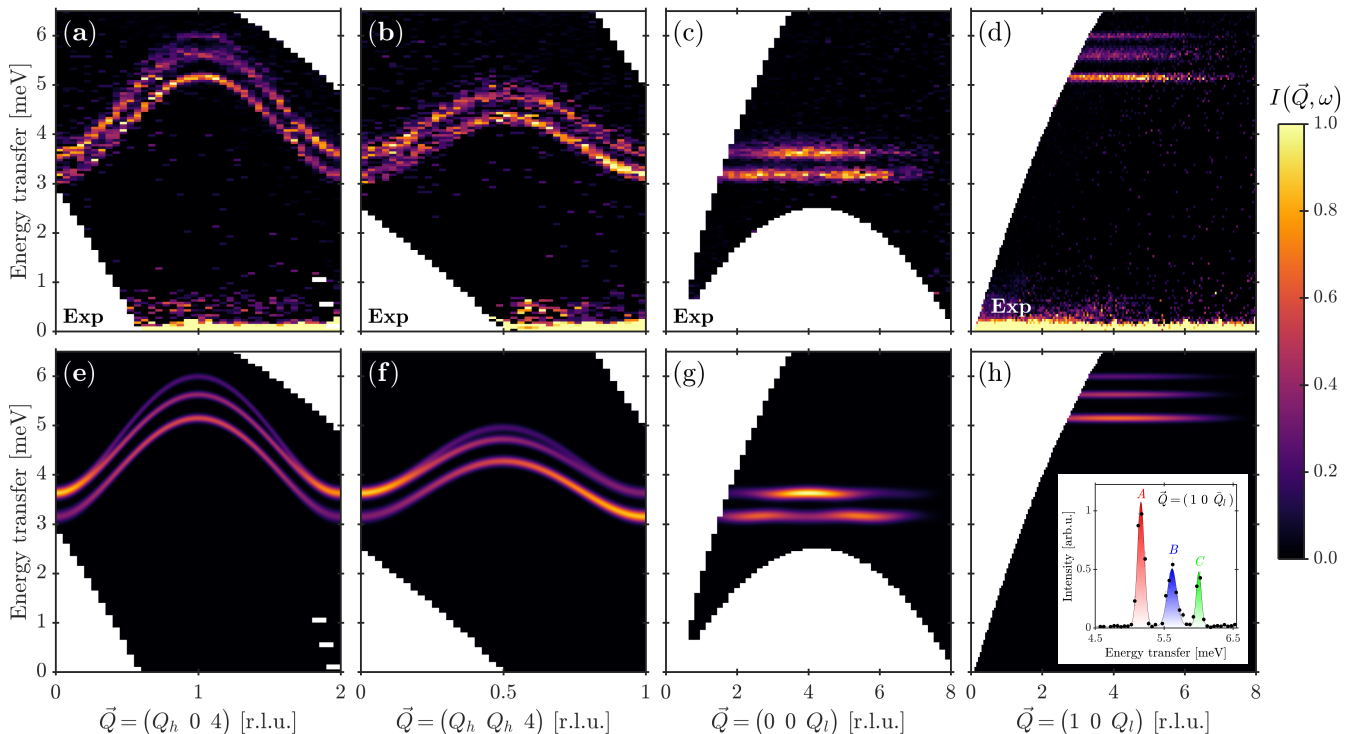


FIG. 2. (a)-(d) Intensity, $I(\vec{Q}, \omega)$, measured on AMATERAS for selected high-symmetry directions. (e)-(h) Corresponding spectra calculated with the fitted interaction parameters. \vec{Q} is indexed in reciprocal lattice units (r.l.u.) of the crystallographic unit cell. Inset in (h) shows the intensity, $I(\omega)$, obtained by integrating over the \vec{Q} ranges $[0.95, 1.05]$ in Q_h , $[-0.05, 0.05]$ in Q_k , and $[4, 8]$ in Q_l (denoted by \vec{Q}_l).

compare our interaction parameters with those deduced from previous INS studies [11, 22] in Sec. S6 of the SM [23].

Returning to the primary experimental observations, (i) the positions of the minima and maxima of the dispersive modes in $(Q_h 0 4)$ and $(Q_h Q_h 4)$ are characteristic of FM effective intra-bilayer interactions. Because each J'_σ is the sum of four inter-ionic interactions, which are generally AF, their sign indicates that the diagonal interactions represented in the inset of Fig. 1(a) are dominant [18]. For effective AF interactions, the positions of the maxima and minima would be exchanged; INS spectra calculated for intra- and inter-bilayer interactions of different signs are shown in Sec. S6 of the SM [23]. We stress again that FM intra-bilayer interactions mean there is no inter-bilayer frustration in $\text{BaCuSi}_2\text{O}_6$.

(ii) While the very weak J'' results in almost flat modes along $(0 0 Q_l)$ [Figs. 2(c) and 3(b)], the mode intensities are Q_l dependent, displaying a double-peak structure in mode A with maxima at $Q_l = 3$ and 5 [Figs. 2(c) and 3(d)]. This feature, which allows us to fit J'' , could not be resolved at all in Ref. [11] and was revealed only by using optimized chopper settings on both high-resolution TOF spectrometers. The fact that the double peak appears in A is a direct consequence of a FM J'' ; an AF inter-bilayer

interaction would cause it to appear in $B+C$ (Sec. S6 of the SM [23]).

(iii) Because the $(1 0 Q_l)$ dispersion [Fig. 2(d)] is Q_l invariant, it is of particular value for a quantitative determination of the relative fractions of each bilayer type. The large detector coverage of LET and AMATERAS allowed us to obtain high-quality data not available in previous experiments [11]. The \vec{Q} -integrated intensity shown in the inset of Fig. 2(h) establishes that the three types of bilayer are present in the approximate ratios $A:B:C = 3:2:1$, as detailed in Sec. S7 of the SM [23]. This information, which makes completely specific the average structure reported in Ref. [16], is the foundation for the *ABABAC* bilayer sequence in the minimal model [Fig. 1(a)]. This model manifestly allows a highly accurate determination of the magnetic interactions and provides an excellent account of the measured spectra, in which neither the very weak orthorhombicity [$b/a = 1.00167(1)$ [16]] nor the incommensurability [12, 19] of the crystal structure plays a role.

The signs and sizes of the interaction parameters we deduce are fully consistent with the *ab initio* analysis [18]. Assuming negligible magnetostriction, these zero-field parameters have immediate consequences for the field-temperature phase diagram and the field-induced

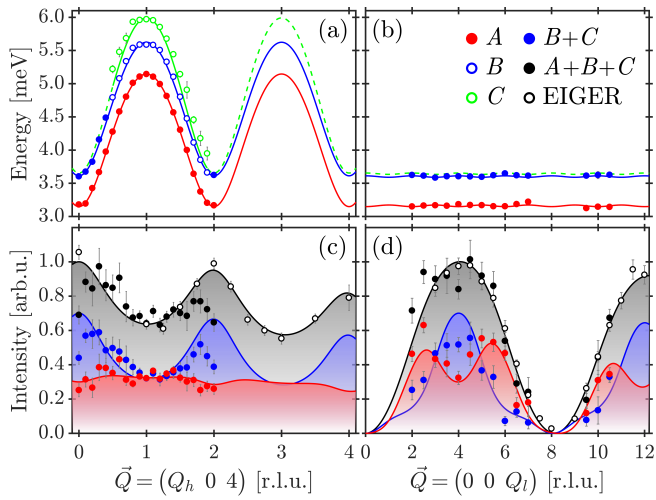


FIG. 3. Mode energies and intensities. All data other than the open circles in (c) and (d) are from AMATERAS. Lines show calculated results; in (a) and (b) the solid blue line represents B , whereas in (c) and (d) it represents the contribution of $B+C$. The dashed green line denotes the energy of C calculated in the range where it was not distinguishable in experiment.

QPT. Based on the initial work of Refs. [43, 44], many authors have discussed their $\text{BaCuSi}_2\text{O}_6$ data [3, 11–13] and models [4, 5, 7, 8, 14, 15, 45] by assuming AF intra-bilayer interactions, and hence strong inter-bilayer frustration, begging the question of how to understand these measurements when frustration is entirely absent. To address this issue in a fully quantitative manner, we perform state-of-the-art stochastic series expansion QMC simulations [46] of the six-bilayer ($ABABAC$) model of Fig. 1 using the interaction parameters we determine by INS.

We simulate an effective Hamiltonian of hard-core bosons [47], to reduce the computational cost, on lattices of size $3L^3$ up to $L = 22$ (equivalent to 63888 spins); details are presented in Sec. S8 of the SM [23]. We calculate the temperature, $T_c(H)$, of the field-induced ordering transition from the scaled spin stiffness, $L^{(d+z-2)}\rho(L, T)$ [48], obtaining complete quantitative agreement with the phase boundary measured in Refs. [3, 12, 43] over the entire range of field-induced magnetic order [Fig. 4(a)]. Here we have fixed $g_{\parallel} = 2.435$ so that the lower critical field is $H_{c1} = 23.4$ T, matching the best estimate available from nuclear magnetic resonance (NMR) [13]. Thus the agreement in Fig. 4(a) is achieved with no adjustable parameters, which, even in comparison with other well-characterized quantum magnets [17], is quite remarkable.

In Fig. 4(b) we show the field-induced triplet densities in all three bilayers at a fixed low temperature of $T = 100$ mK. Clearly the A -bilayer density, ρ_A , rises rapidly and near-linearly in $h = H - H_{c1}$, whereas ρ_B and ρ_C rise slowly with leading linear and quadratic components, in

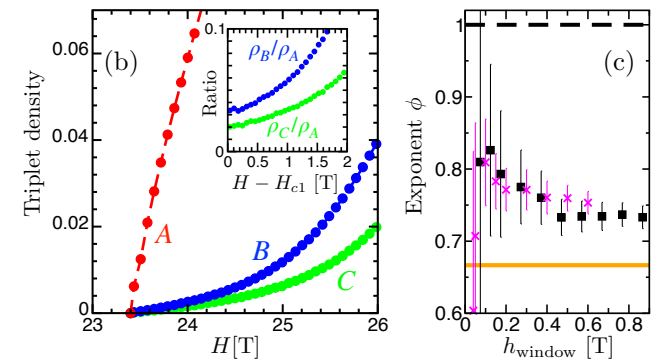
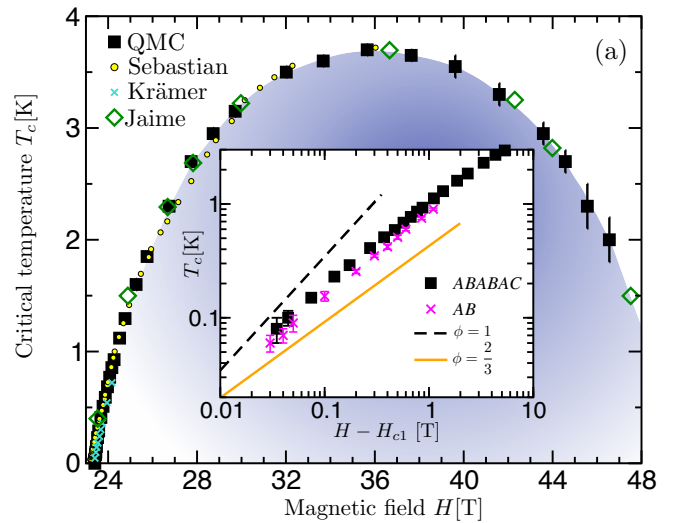


FIG. 4. QMC results for the $ABABAC$ model. (a) (H, T) phase diagram of the field-induced ordered regime, compared with experimental data from Refs. [3, 12, 43]. (Inset) Power-law scaling obtained for $ABABAC$ and AB models (see text) and compared with the scaling forms of pure 2D ($\phi = 1$) and 3D ($\phi = 2/3$) criticality. (b) Triplet populations in the three types of bilayer, computed for 1536 dimer units and shown as a function of field at $T = 100$ mK. (Inset) Population ratios. (c) Effective exponent, ϕ , extracted from power-law fits of the QMC data [inset (a)] to a window of width h_{window} .

agreement with the NMR determination of ρ_A and ρ_B [13]. The magnetic order parameter is determined by the effective triplet tunnelling between the A bilayers, $t_{3D}^{\text{eff}}(h)$, which is limited by the low triplet densities in the B and C bilayers (whose individual gaps have not yet closed). At low densities, $t_{3D}^{\text{eff}}(h)$ is proportional to the ratios $r_{BA} = \rho_B/\rho_A$ and r_{CA} [14], and thus close to H_{c1} takes the generic form

$$t_{3D}^{\text{eff}}(h) = t_c^{\text{eff}} + a_1 h + a_2 h^2 + O(h^3). \quad (1)$$

r_{BA} and r_{CA} grow smoothly at $H > H_{c1}$ [inset, Fig. 4(b)] and, crucially, remain finite at $H = H_{c1}$, giving a finite t_c^{eff} (which is the case for any incomplete frustration [8, 13, 15]). Thus as $h \rightarrow 0$, the condensed triplets have a strongly anisotropic but 3D dispersion and the criti-

cal behavior of the phase boundary is described by the exponent $\phi = z/d = 2/3$ of a fully 3D QPT.

However, the structural modulation introduces a new energy scale, $J_B - J_A$, and with it an energy scale $(J'')^2/(J_B - J_A)$ [14]. Temperatures above this latter scale (approximately 0.04 K) may act to decouple the A bilayers, leading to an anomalous effective exponent, $\phi(h)$, over a range of h . This is corroborated by our QMC results for $T_c(H)$ in the candidate quantum critical regime [inset, Fig. 4(a)], both for the $ABABAC$ model of $\text{BaCuSi}_2\text{O}_6$ and for a simplified two-layer AB model giving access to lower temperatures. We extract an effective ϕ by power-law fits in a window of width h_{window} and find [Fig. 4(c)] that it does not show accurate 3D scaling for any realistic h_{window} , but also never approaches 2D scaling. Only for $h_{\text{window}} < 0.08$ T do our AB-model data suggest that the genuine 3D critical scaling regime is entered. Above this we demonstrate a clear crossover into an additional regime of non-trivial effective scaling, arising due to bilayer modulation, in which $\phi(h)$ is determined by the field-evolution of $t_{3D}^{\text{eff}}(h)$.

We therefore verify that the $ABABAC$ model with an unfrustrated inter-bilayer interaction is fully consistent with all of the previous, highly detailed experiments that have probed the properties of $\text{BaCuSi}_2\text{O}_6$ [3, 11–13, 16, 19–21, 42–44]. The appearance of dimensional reduction near the QPT [3] is a consequence only of the inequivalent bilayer units and not of frustration [8]. The unconventional physics in this previously unrecognized regime is contained in the effective triplet tunnelling between A bilayers [Eq. (1)], where $t_c^{\text{eff}} \neq 0$ ensures both a finite (if narrow) regime of 3D scaling (the true QPT is always 3D) and a non-universal, window-dependent scaling regime with $2/3 < \phi < 1$. With rapidly improving technological capabilities for building atomically layered magnetic materials [49–54], this type of knowledge concerning emergent behavior due to layer modulation will be essential to the design of their physical properties.

In summary, we report high-resolution INS measurements over the full band width of the magnetic excitations in $\text{BaCuSi}_2\text{O}_6$. We have determined the minimal magnetic Hamiltonian required to model the spectrum and find that it contains three different bilayer types in the ratios 3:2:1. We verify that the effective intra-bilayer interaction parameters are ferromagnetic, which precludes any inter-bilayer frustration. We perform QMC simulations of the full magnetic model to demonstrate that our parameters account with quantitative accuracy both for the entire (H, T) phase boundary and for its anomalous scaling within a window of width 1 K near the QPT.

Acknowledgments. We thank S. Sebastian and I. Fisher for providing large, high-quality single-crystal samples and F. Giorgianni, M. Horvatić, P. Puphal, D. Sheptyakov, R. Stern and S. Ward for helpful discussions. N.L. and F.M. are also indebted to

C. Berthier and S. Krämer for an earlier collaboration on this material. This work is based in part on experiments performed at the Swiss Spallation Neutron Source SINQ at the Paul Scherrer Institute. Measurements on AMATERAS were performed based on the approved proposal No. 2015A0320. Experiments at the ISIS Pulsed Neutron and Muon Source were supported by a beam time allocation from the Science and Technology Facilities Council. We thank the Swiss National Science Foundation and the ERC Grant Hyper Quantum Criticality (HyperQC) for financial support. N.L. thanks the French National Research Agency (ANR) for support under project THERMOLOC ANR-16-CE30-0023-0. We acknowledge CALMIP (Grants No. 2018-P0677 and No. 2019-P0677) and GENCI (Grant No. 2018-A0030500225) for high-performance computing resources.

-
- [1] Jean Zinn-Justin, *Quantum Field Theory and Critical Phenomena* (Clarendon Press, Oxford, 2002).
 - [2] S. Sachdev, *Quantum Phase Transitions* (Cambridge University Press, Cambridge, England, 2011).
 - [3] S. E. Sebastian, N. Harrison, C. D. Batista, L. Balicas, M. Jaime, P. A. Sharma, N. Kawashima, and I. R. Fisher, “Dimensional reduction at a quantum critical point,” *Nature (London)* **441**, 617 (2006).
 - [4] C. D. Batista, J. Schmalian, N. Kawashima, P. Sengupta, S. E. Sebastian, N. Harrison, M. Jaime, and I. R. Fisher, “Geometric Frustration and Dimensional Reduction at a Quantum Critical Point,” *Phys. Rev. Lett.* **98**, 257201 (2007).
 - [5] J. Schmalian and C. D. Batista, “Emergent symmetry and dimensional reduction at a quantum critical point,” *Phys. Rev. B* **77**, 094406 (2008).
 - [6] M. Maltseva and P. Coleman, “Failure of geometric frustration to preserve a quasi-two-dimensional spin fluid,” *Phys. Rev. B* **72**, 174415 (2005).
 - [7] O. Rösch and M. Vojta, “Quantum phase transitions and dimensional reduction in antiferromagnets with interlayer frustration,” *Phys. Rev. B* **76**, 180401 (2007).
 - [8] O. Rösch and M. Vojta, “Reduced dimensionality in layered quantum dimer magnets: Frustration vs. inhomogeneous condensates,” *Phys. Rev. B* **76**, 224408 (2007).
 - [9] L. W. Finger, R. M. Hazen, and R. J. Hemley, “ $\text{BaCuSi}_2\text{O}_6$: A new cyclosilicate with four-membered tetrahedral rings,” *Am. Miner.* **74**, 952 (1989).
 - [10] Elisabeth West FitzHugh and Lynda A. Zycherman, “A purple barium copper silicate pigment from early China,” *Stud. Conserv.* **37**, 145 (1992).
 - [11] Ch. Rüegg, D. F. McMorrow, B. Normand, H. M. Rønnow, S. E. Sebastian, I. R. Fisher, C. D. Batista, S. N. Gvasaliya, Ch. Niedermayer, and J. Stahn, “Multiple Magnon Modes and Consequences for the Bose-Einstein Condensed Phase in $\text{BaCuSi}_2\text{O}_6$,” *Phys. Rev. Lett.* **98**, 017202 (2007).
 - [12] S. Krämer, R. Stern, M. Horvatić, C. Berthier, T. Kimura, and I. R. Fisher, “Nuclear magnetic resonance evidence for a strong modulation of the Bose-

- Einstein condensate in $\text{BaCuSi}_2\text{O}_6$,” *Phys. Rev. B* **76**, 100406 (2007).
- [13] S. Krämer, N. Laflorencie, R. Stern, M. Horvatić, C. Berthier, H. Nakamura, T. Kimura, and F. Mila, “Spatially resolved magnetization in the Bose-Einstein condensed state of $\text{BaCuSi}_2\text{O}_6$: Evidence for imperfect frustration,” *Phys. Rev. B* **87**, 180405 (2013).
- [14] N. Laflorencie and F. Mila, “Theory of the Field-Induced BEC in the Frustrated Spin- $\frac{1}{2}$ Dimer Compound $\text{BaCuSi}_2\text{O}_6$,” *Phys. Rev. Lett.* **102**, 060602 (2009).
- [15] N. Laflorencie and F. Mila, “Condensate-Free Superfluid Induced by the Frustrated Proximity Effect,” *Phys. Rev. Lett.* **107**, 037203 (2011).
- [16] D. V. Sheptyakov, V. Yu. Pomjakushin, R. Stern, I. Heinmaa, H. Nakamura, and T. Kimura, “Two types of adjacent dimer layers in the low-temperature phase of $\text{BaCuSi}_2\text{O}_6$,” *Phys. Rev. B* **86**, 014433 (2012).
- [17] V. Zapf, M. Jaime, and C. D. Batista, “Bose-Einstein condensation in quantum magnets,” *Rev. Mod. Phys.* **86**, 563 (2014).
- [18] V. V. Mazurenko, M. V. Valentyuk, R. Stern, and A. A. Tsirlin, “Nonfrustrated Interlayer Order and its Relevance to the Bose-Einstein Condensation of Magnons in $\text{BaCuSi}_2\text{O}_6$,” *Phys. Rev. Lett.* **112**, 107202 (2014).
- [19] E. C. Samulon, Z. Islam, S. E. Sebastian, P. B. Brooks, M. K. McCourt, J. Ilavsky, and I. R. Fisher, “Low-temperature structural phase transition and incommensurate lattice modulation in the spin-gap compound $\text{BaCuSi}_2\text{O}_6$,” *Phys. Rev. B* **73**, 100407 (2006).
- [20] K. Röwer, M. Merz, G. Roth, R. Stern, R. Cerny, and T. Kimura, “Low temperature phase transition in $\text{BaCuSi}_2\text{O}_6$,” *Acta Cryst. A* **62**, 197 (2006).
- [21] R. Stern, I. Heinmaa, E. Joon, A. A. Tsirlin, H. Nakamura, and T. Kimura, “Low-Temperature High-Resolution Solid-State (cryoMAS) NMR of Han Purple $\text{BaCuSi}_2\text{O}_6$,” *Appl. Magn. Reson.* **45**, 1253 (2014).
- [22] Y. Sasago, K. Uchinokura, A. Zheludev, and G. Shirane, “Temperature-dependent spin gap and singlet ground state in $\text{BaCuSi}_2\text{O}_6$,” *Phys. Rev. B* **55**, 8357 (1997).
- [23] See Supplemental Material, which includes Refs. [24–36], for details of the sample, unit-cell definitions, data modelling, the magnetic form factor, the relative bilayer fractions, and the quantum Monte Carlo simulations.
- [24] O. Arnold, J. C. Bilheux, J. M. Borreguero, A. Buts, S. I. Campbell, L. Chapon, M. Doucet, N. Draper, R. Ferraz Leal, M. A. Gigg, V. E. Lynch, A. Markvardsen, D. J. Mikkelsen, R. L. Mikkelsen, R. Miller, K. Palmen, P. Parker, G. Passos, T. G. Perring, P. F. Peterson, S. Ren, M. A. Reuter, A. T. Savici, J. W. Taylor, R. J. Taylor, R. Tolchenov, W. Zhou, and J. Zikovsky, “Mantid – Data analysis and visualization package for neutron scattering and μSR experiments,” *Nucl. Instrum. Methods Phys. Res., Sect. A* **764**, 156 (2014).
- [25] Y. Inamura, T. Nakatani, J. Suzuki, and T. Otomo, “Development status of software “Utsusemi” for Chopper Spectrometers at MLF, J-PARC,” *J. Phys. Soc. Jpn.* **82**, SA031 (2013).
- [26] R. A. Ewings, A. Buts, M. D. Le, J. van Duijn, I. Bustinduy, and T. G. Perring, “Horace: Software for the analysis of data from single crystal spectroscopy experiments at time-of-flight neutron instruments,” *Nucl. Instrum. Methods Phys. Res., Sect. A* **834**, 132 (2016).
- [27] S. B. Haley and P. Erdős, “Standard-Basis Operator Method in the Green’s-Function Technique of Many-Body Systems with an Application to Ferromagnetism,” *Phys. Rev. B* **5**, 1106 (1972).
- [28] B. Normand and Ch. Rüegg, “Complete bond-operator theory of the two-chain spin ladder,” *Phys. Rev. B* **83**, 054415 (2011).
- [29] M. Matsumoto, B. Normand, T. M. Rice, and M. Sigrist, “Field- and pressure-induced magnetic quantum phase transitions in TlCuCl_3 ,” *Phys. Rev. B* **69**, 054423 (2004).
- [30] A. Furrer, J. Mesot, and T. Strässle, *Neutron Scattering in Condensed Matter Physics* (World Scientific, Singapore, 2009).
- [31] E. Prince, *International Tables for Crystallography. Volume C: Mathematical, Physical and Chemical Tables* (Kluwer Academic Publishers, Dordrecht, 2004).
- [32] R. Coldea, S. M. Hayden, G. Aeppli, T. G. Perring, C. D. Frost, T. E. Mason, S.-W. Cheong, and Z. Fisk, “Spin Waves and Electronic Interactions in La_2CuO_4 ,” *Phys. Rev. Lett.* **86**, 5377 (2001).
- [33] N. S. Headings, S. M. Hayden, R. Coldea, and T. G. Perring, “Anomalous High-Energy Spin Excitations in the High- T_c Superconductor-Parent Antiferromagnet La_2CuO_4 ,” *Phys. Rev. Lett.* **105**, 247001 (2010).
- [34] I. A. Zaliznyak, H. Woo, T. G. Perring, C. L. Broholm, C. D. Frost, and H. Takagi, “Spinons in the Strongly Correlated Copper Oxide Chains in SrCuO_2 ,” *Phys. Rev. Lett.* **93**, 087202 (2004).
- [35] A. C. Walters, T. G. Perring, J.-S. Caux, A. T. Savici, G. D. Gu, C.-C. Lee, W. Ku, and I. A. Zaliznyak, “Effect of covalent bonding on magnetism and the missing neutron intensity in copper oxide compounds,” *Nat. Phys.* **5**, 867 (2009).
- [36] M. Campostrini, A. Pelissetto, P. Rossi, and E. Vicari, “Determination of the critical exponents for the λ transition of ^4He by high-temperature expansion,” *Phys. Rev. B* **61**, 5905 (2000).
- [37] K. Nakajima, S. Ohira-Kawamura, T. Kikuchi, M. Nakamura, R. Kajimoto, Y. Inamura, N. Takahashi, K. Aizawa, K. Suzuya, K. Shibata, T. Nakatani, K. Soyama, R. Maruyama, H. Tanaka, W. Kambara, T. Iwahashi, Y. Itoh, T. Osakabe, S. Wakimoto, and M. Arai, “AMATERAS : A Cold-Neutron Disk Chopper Spectrometer,” *J. Phys. Soc. Jpn.* **80**, SB028 (2011).
- [38] R. I. Bewley, J. W. Taylor, and S. M. Bennington, “LET, a cold neutron multi-disk chopper spectrometer at ISIS,” *Nucl. Instrum. Methods Phys. Res., Sect. A* **637**, 128 (2011).
- [39] U. Stuhr, B. Roessli, S. Gvasaliya, H. M. Rønnow, U. Filges, D. Graf, A. Bollhalder, D. Hohl, R. Bürge, M. Schild, L. Holitzner, C. Kägi, P. Keller, and T. Mühlebach, “The thermal triple-axis-spectrometer EIGER at the continuous spallation source SINQ,” *Nucl. Instrum. Methods Phys. Res., Sect. A* **853**, 16 (2017).
- [40] B. Leuenberger, H.-U. Güdel, R. Feile, and J. K. Kjems, “Collective excitations in the singlet-ground-state dimer system $\text{Cs}_3\text{Cr}_2\text{Br}_9$,” *Phys. Rev. B* **28**, 5368 (1983).
- [41] B. Leuenberger, A. Stebler, H.-U. Güdel, A. Furrer, R. Feile, and J. K. Kjems, “Spin dynamics of an isotropic singlet-ground-state antiferromagnet with alternating strong and weak interactions: An inelastic-neutron-scattering study of the dimer compound $\text{Cs}_3\text{Cr}_2\text{Br}_9$,” *Phys. Rev. B* **30**, 6300 (1984).
- [42] S. Zvyagin, J. Wosnitzer, J. Krzystek, R. Stern, M. Jaime, Y. Sasago, and K. Uchinokura, “Spin-triplet excitons in the $S = 1/2$ gapped antiferromagnet $\text{BaCuSi}_2\text{O}_6$: Elec-

- tron paramagnetic resonance studies,” *Phys. Rev. B* **73**, 094446 (2006).
- [43] M. Jaime, V. F. Correa, N. Harrison, C. D. Batista, N. Kawashima, Y. Kazuma, G. A. Jorge, R. Stern, I. Heinmaa, S. A. Zvyagin, Y. Sasago, and K. Uchinokura, “Magnetic-Field-Induced Condensation of Triplons in Han Purple Pigment $\text{BaCuSi}_2\text{O}_6$,” *Phys. Rev. Lett.* **93**, 087203 (2004).
- [44] S. E. Sebastian, P. A. Sharma, M. Jaime, N. Harrison, V. Correa, L. Balicas, N. Kawashima, C. D. Batista, and I. R. Fisher, “Characteristic Bose-Einstein condensation scaling close to a quantum critical point in $\text{BaCuSi}_2\text{O}_6$,” *Phys. Rev. B* **72**, 100404 (2005).
- [45] Y. Kamiya, N. Kawashima, and C. D. Batista, “Finite-Temperature Transition in the Spin-Dimer Antiferromagnet $\text{BaCuSi}_2\text{O}_6$,” *J. Phys. Soc. Jpn.* **78**, 094008 (2009).
- [46] Olav F. Syljuåsen and Anders W. Sandvik, “Quantum Monte Carlo with directed loops,” *Phys. Rev. E* **66**, 046701 (2002).
- [47] F. Mila, “Ladders in a magnetic field: a strong coupling approach,” *Eur. Phys. J. B* **6**, 201 (1998).
- [48] A. W. Sandvik, “Critical Temperature and the Transition from Quantum to Classical Order Parameter Fluctuations in the Three-Dimensional Heisenberg Antiferromagnet,” *Phys. Rev. Lett.* **80**, 5196 (1998).
- [49] M. Gibertini, M. Koperski, A. F. Morpurgo, and K. S. Novoselov, “Magnetic 2D materials and heterostructures,” *Nat. Nanotechnol.* **14**, 408 (2019).
- [50] D. R. Klein, D. MacNeill, Q. Song, D. T. Larson, S. Fang, M. Xu, R. A. Ribeiro, P. C. Canfield, E. Kaxiras, R. Comin, and P. Jarillo-Herrero, “Enhancement of interlayer exchange in an ultrathin 2D magnet,” *Nat. Phys.* **15**, 1255 (2019).
- [51] N. Ubrig, Z. Wang, J. Teyssier, T. Taniguchi, K. Watanabe, E. Giannini, A. F. Morpurgo, and M. Gibertini, “Low-temperature monoclinic layer stacking in atomically thin CrI_3 crystals,” *2D Mater.* **7**, 015007 (2019).
- [52] X. Cai, T. Song, N. P. Wilson, G. Clark, M. He, X. Zhang, T. Taniguchi, K. Watanabe, W. Yao, D. Xiao, M. A. McGuire, D. H. Cobden, and X. Xu, “Atomically Thin CrCl_3 : An In-Plane Layered Antiferromagnetic Insulator,” *Nano Lett.* **19**, 3993 (2019).
- [53] Z. Wang, M. Gibertini, D. Dumcenco, T. Taniguchi, K. Watanabe, E. Giannini, and A. F. Morpurgo, “Determining the phase diagram of the atomically thin layered antiferromagnet CrCl_3 ,” *Nat. Nanotechnol.* **14**, 1116 (2019).
- [54] H. H. Kim, B. Yang, S. Li, S. Jiang, C. Jin, Z. Tao, G. Nichols, F. Sfigakis, S. Zhong, C. Li, S. Tian, D. G. Cory, G.-X. Miao, J. Shan, K. F. Mak, H. Lei, K. Sun, L. Zhao, and A. W. Tsun, “Evolution of interlayer and intralayer magnetism in three atomically thin chromium trihalides,” *Proc. Natl. Acad. Sci. U.S.A.* **116**, 11131 (2019).

Supplemental Material for “Multiple Magnetic Bilayers and Unconventional Criticality without Frustration in BaCuSi₂O₆”

S. Allenspach, A. Biffin, U. Stuhr, G. S. Tucker, S. Ohira-Kawamura, M. Kofu, D. J. Voneshen, M. Boehm, B. Normand, N. Laflorencie, F. Mila, and Ch. Rüegg

S1. BASIS TRANSFORMATION BETWEEN UNIT CELLS

As stated in the main text, using the crystallographic unit cell of BaCuSi₂O₆ creates an ambiguity in the interpretation of observed triplon dispersions. In brief, doubling of the spatial unit cell creates two excitation branches in the halved Brillouin zone, which have complementary energy minima and maxima. Here we present the transformation between the basis $\{\hat{a}, \hat{b}, \hat{c}\}$ of the orthorhombic crystallographic unit cell of the low-temperature structure, as reported in Ref. [16], and basis $\{\hat{a}', \hat{b}', \hat{c}'\}$ of the unit cell of the minimal model shown in Fig. 1 of the main text. These differ not only in the plane of the bilayer [Fig. 1(b)] but also in the number of bilayers in a cell (respectively 4 and 6).

The c and c' axes are both perpendicular to the bilayers. We define the quantity d_{bl} for the separation of neighboring bilayers, whence

$$c = |\vec{c}| = 4d_{\text{bl}} \quad \text{and} \quad c' = |\vec{c}'| = 6d_{\text{bl}}. \quad (\text{S1})$$

The basis vectors of the minimal and crystallographic unit cells in the plane of the bilayers are related by

$$\vec{a} = \vec{b}' + \vec{a}' \quad \text{and} \quad \vec{b} = \vec{b}' - \vec{a}'. \quad (\text{S2})$$

The transformation of coordinates in reciprocal space is then given by

$$Q_h = Q'_h + Q'_k, \quad Q_k = Q'_k - Q'_h, \quad Q_l = \frac{2}{3}Q'_l \quad (\text{S3})$$

and the inverted form

$$Q'_h = \frac{1}{2}(Q_h - Q_k), \quad Q'_k = \frac{1}{2}(Q_h + Q_k), \quad Q'_l = \frac{3}{2}Q_l. \quad (\text{S4})$$

We note that using a tetragonal crystallographic unit cell results in the same transformation. We refer to \vec{Q} as the “crystallographic basis” and to \vec{Q}' as the “minimal basis.” In the halved Brillouin zone of each bilayer in the crystallographic basis, the second triplon mode is phase-shifted by half a period and is actually a “shadow mode” with no intensity, but further analysis is required to establish which mode is the “real” one.

S2. SINGLE-CRYSTAL SAMPLE

For the experimental measurements on all spectrometers we used the same flux-grown single crystal, which

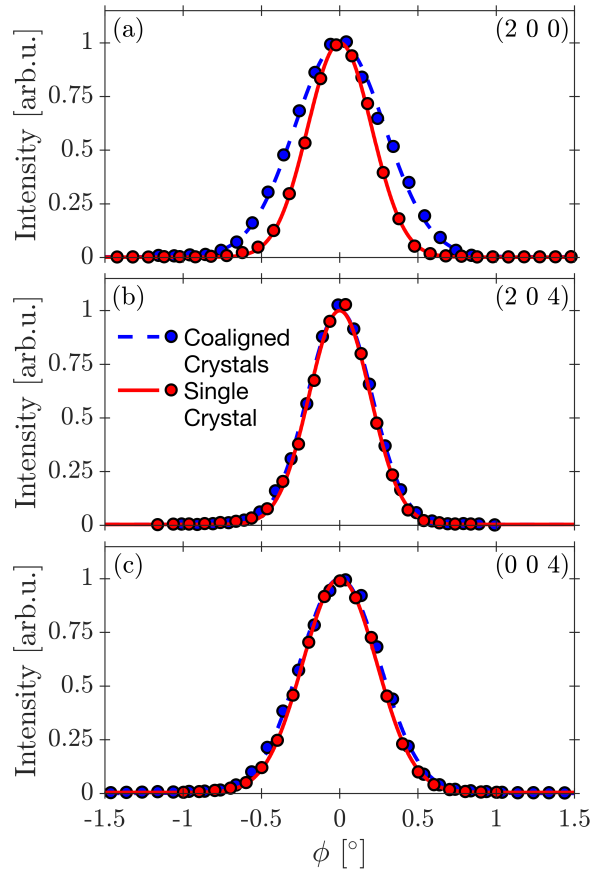


FIG. S1. Rocking curves across three Bragg peaks of the single-crystalline BaCuSi₂O₆ sample (solid red lines), which are (a) (2 0 0), (b) (2 0 4), and (c) (0 0 4) in the crystallographic basis. Shown for comparison are rocking curves obtained with the same instrument settings for the coaligned sample of five small single crystals used in Ref. [11]. The intensities of all peaks have been scaled to unity.

was oblate in form and had a mass of 1.01 g. The growth method and basic characterization information are presented in Ref. [44]. For the purposes of a scattering experiment, we measured the mosaic spread of the crystal at room temperature on the two-axis diffractometer MORPHEUS at the SINQ neutron source; the same procedure was employed to characterize the sample used in Ref. [11], which consisted of five smaller coaligned crystals with a total mass of 1.25 g. Figure S1 shows rocking curves across two Bragg peaks for both samples. These scans were performed with the same resolution settings in both cases, in order to be able to compare the peak

shapes, but we caution that these were not precisely the same settings used in Fig. 2(a) of Ref. [11]. While Fig. S1 indicates that the structural quality of the single-crystal sample is slightly superior to that of the coaligned one, additional advantages for INS purposes include its compact nature and no aluminium holder, all of which resulted in significant improvements in energy and wave-vector resolution.

S3. DATA PRE-PROCESSING

Raw TOF data from LET were pre-processed using the software Mantid [24] and data from AMATERAS using Utsusemi [25]. On LET, the raw data were normalized to a vanadium standard and an empty-can measurement was subtracted. The software package Horace [26] was then used to create ‘‘cuts’’ in wave vector, \vec{Q} , and energy transfer, ω , from the four-dimensional dataset. All data gathered on both ToF and triple-axis instruments were multiplied by the factor k_i/k_f to obtain the intensities, $I(\vec{Q}, \omega)$, presented in Figs. 2(a)-2(d) and 3 of the main text.

To analyze the ToF data, we prepared cuts as a function of ω for sets of \vec{Q} points along selected high-symmetry directions. These cuts displayed two or three independent excitation peaks, depending on whether modes B and C were distinguishable at the relevant \vec{Q} , which were fitted with the corresponding number of Gaussian functions plus a background contribution. In Fig. 3 of the main text, the maxima of the Gaussians are taken to define the mode energies and their weights as the mode intensities.

S4. MODELING THE SPECTRUM

It is clear both from the structure of $\text{BaCuSi}_2\text{O}_6$ [16] and from earlier experimental results [11] that there exist at least two different dimer types in the unit cell, or dimer sublattices within the system. Dimers in separate sublattices have different intradimer interaction parameters, and presumably also different interdimer (but intra-sublattice) ones. To calculate the magnetic excitation spectrum under these circumstances we consider an arbitrary dimerized $S = 1/2$ spin system with only Heisenberg interactions.

The magnetic Hamiltonian can be expressed as

$$\begin{aligned} \hat{\mathcal{H}} &= \hat{\mathcal{H}}_{\text{intra}} + \hat{\mathcal{H}}_{\text{inter}} \\ &= \sum_{n,\sigma} J_{n\sigma} \hat{\mathbf{S}}_{n\sigma 1} \cdot \hat{\mathbf{S}}_{n\sigma 2} + \sum'_{nm,\sigma\rho,pr} \frac{1}{2} J'_{n\sigma p, m\rho r} \hat{\mathbf{S}}_{n\sigma p} \cdot \hat{\mathbf{S}}_{m\rho r}, \end{aligned} \quad (\text{S5})$$

in which $\hat{\mathbf{S}}_{n\sigma p}$ is the operator for the ionic spin on a single site, m and n label separate unit cells, σ and ρ label

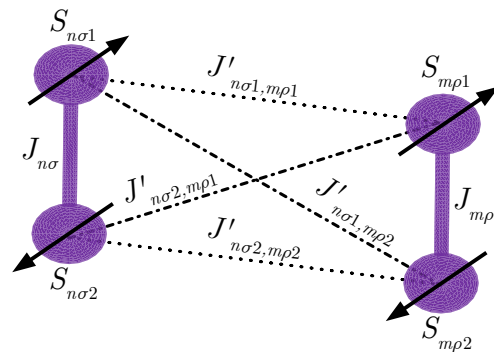


FIG. S2. Schematic representation of the interaction pathways between two pairs of dimerized $S = 1/2$ ions. Arrows represent instantaneous relative spin orientations for all-AF Heisenberg interactions obeying $J_{n\sigma}, J_{m\rho} > J'_{n\sigma 1, m\rho 2}, J'_{n\sigma 2, m\rho 1} > J'_{n\sigma 1, m\rho 1}, J'_{n\sigma 2, m\rho 2}$.

the dimer sublattice within a unit cell, $p, r \in \{1, 2\}$ label the two ions making up each dimer, and the second sum excludes the term $n\sigma = m\rho$ (which is in fact the first sum). The eigenbasis of $\hat{\mathcal{H}}_{\text{intra}}$ consists only of the singlet and triplet eigenstates of a single dimer, whose total occupations must sum to unity. Because there is no external magnetic field, the three triplet modes are degenerate at all times. The starting condition that the dimer bonds, $J_{n\sigma}$, are AF and the strongest interactions in the system ensures that the problem is reduced to the dynamics of a very low density of triplets moving in a singlet background. As represented in Fig. S2, the effective interdimer hopping of these triplon quasiparticles is given in terms of the ionic interactions of Eq. (S5) by

$$J'_{n\sigma, m\rho} = \frac{1}{2} (J'_{n\sigma 1, m\rho 1} - J'_{n\sigma 1, m\rho 2} - J'_{n\sigma 2, m\rho 1} + J'_{n\sigma 2, m\rho 2}). \quad (\text{S6})$$

Clearly in the case of the intra-bilayer interactions labeled J'_σ ($\sigma = A, B, C$) in Fig. 1(a) of the main text, the effectively FM sign of these parameters results from AF ionic interaction terms satisfying $J'_{n\sigma 1, m\rho 2} = J'_{n\sigma 2, m\rho 1} > J'_{n\sigma 1, m\rho 1} = J'_{n\sigma 2, m\rho 2}$ [18]. We comment that the inter-bilayer term, J'' , is treated as a single, ionic interaction (Fig. 1(a) of the main text), and hence the sign of this parameter is in fact the consequence of a genuinely FM superexchange process.

To discuss the triplet dynamics, we generalized the Green-function approach of Refs. [40, 41], which for any number, N , of sublattices provides $2N$ independent coupled equations for diagonal and off-diagonal processes in the triplet occupation basis, but does not mix triplet modes at different wave vectors, \vec{K} [27]. Assuming at zero temperature that the singlet and triplet occupation probabilities on every dimer obey $\langle \hat{n}_s^\sigma \rangle + 3\langle \hat{n}_t^\sigma \rangle = 1$ is an approximation entirely equivalent to using the bond-operator approach [28] in the Holstein-Primakoff approx-

imation [29]. The poles of the Green function yield the triplon dispersion relations for each \vec{K} .

We restrict our considerations to spin dimer systems, as described by the Hamiltonian of Eq. (S5), but with only one dimer type in each bilayer, because structures involving different dimer types in the same bilayer would exhibit spectra completely different from those observed in experiment. In the remainder of this section we use \vec{K} to denote the wave vector of a general bilayer dimer system and connect our expressions to BaCuSi₂O₆ at the end. For a system with only one dimer type ($\sigma = A$), one obtains

$$\omega_A(\vec{K}) = \sqrt{J_A^2 + J_A J_{AA}(\vec{K})}, \quad (\text{S7})$$

where $J_{AA}(\vec{K})$ is obtained from the terms appearing in Eq. (S6) under Fourier transformation of $\hat{\mathcal{H}}$. With two dimer bilayers ($\sigma = A$ and $\rho = B$), the dispersion relations are

$$\omega_{\pm}(\vec{K}) = \sqrt{\frac{1}{2}[\omega_A^2(\vec{K}) + \omega_B^2(\vec{K}) \pm \mathcal{J}(\vec{K})]} \quad (\text{S8})$$

with

$$\mathcal{J}(\vec{K}) = \sqrt{[\omega_A^2(\vec{K}) - \omega_B^2(\vec{K})]^2 + 4J_A J_B J_{AB}^2(\vec{K})}, \quad (\text{S9})$$

in which we use $\omega_A(\vec{K})$ and $\omega_B(\vec{K})$ from Eq. (S7) for brevity. For more than two dimer sublattices, the polynomial expression has a degree higher than four and it is more convenient to find its roots numerically.

The explicit forms of the functions $J_{\sigma\rho}(\vec{K})$ in these expressions are written most easily by separating intra- and inter-bilayer interaction terms. The intra-bilayer terms in a two-bilayer model ($\sigma \in \{A, B\}$) are given by

$$J_{\sigma\sigma}(\vec{K}) = 2J'_{\sigma}[\cos(2\pi K_h) + \cos(2\pi K_k)], \quad (\text{S10})$$

while the inter-bilayer term for adjacent bilayers of types $\sigma = A$ and $\rho = B$ is

$$J_{AB}(\vec{K}) = -4J'' \cos(\pi K_h) \cos(\pi K_k) \cos(\pi K_l). \quad (\text{S11})$$

By constructing the generalized susceptibility tensor [30] from the triplon Green functions [41], one obtains the magnetic dynamical structure factor at zero temperature, which for a system with one dimer type is given by

$$\mathcal{S}^{\alpha\beta}(\vec{K}, \omega) = N\delta^{\alpha\beta} [f_A(\vec{K})/\omega_A(\vec{K})] \delta(\omega - \omega_A(\vec{K})), \quad (\text{S12})$$

where $f_A(\vec{K}) = J_A[1 - \cos(\vec{K} \cdot \vec{R}_A)]$, with \vec{R}_A the vector connecting the ions of dimer A . For a system with two dimer bilayers,

$$\begin{aligned} \mathcal{S}^{\alpha\beta}(\vec{K}, \omega) &= \frac{1}{4}N\delta^{\alpha\beta} [f_A(\vec{K}) + f_B(\vec{K})] \quad (\text{S13}) \\ &\times \left[(1 + \Xi(\vec{K})) \frac{\delta(\omega - \omega_+(\vec{K}))}{\omega_+(\vec{K})} + (1 - \Xi(\vec{K})) \frac{\delta(\omega - \omega_-(\vec{K}))}{\omega_-(\vec{K})} \right], \end{aligned}$$

where

$$\Xi(\vec{K}) = \frac{[f_A(\vec{K}) - f_B(\vec{K})][\omega_A^2(\vec{K}) - \omega_B^2(\vec{K})] + f_{AB}(\vec{K})}{[f_A(\vec{K}) + f_B(\vec{K})]\mathcal{J}(\vec{K})} \quad (\text{S14})$$

with

$$f_{AB}(\vec{K}) = 8J_A J_B \sin\left(\frac{1}{2}\vec{K} \cdot \vec{R}_A\right) \sin\left(\frac{1}{2}\vec{K} \cdot \vec{R}_B\right) J_{AB}(\vec{K}). \quad (\text{S15})$$

In Eq. (S13), $\omega_{\pm}(\vec{K})$ is given in Eq. (S8) and we show only the part of the dynamical structure factor resulting from excitation processes with positive energy transfer [$\omega(\vec{K}) > 0$].

For a system with more than two bilayer types, which includes the case of BaCuSi₂O₆ (Fig. 1 of the main text), the analytical expression is too cumbersome to be useful and we employ a numerical procedure to construct $\mathcal{S}^{\alpha\beta}(\vec{K}, \omega)$ for every point \vec{K} . We performed these calculations using the minimal basis, \vec{Q}' in Sec. S1, but for historical and experimental consistency we show all our results in the crystallographic basis, \vec{Q} . When the illustrative calculations above are extended to the minimal $ABABAC$ model for BaCuSi₂O₆, the dispersion relations shown in Figs. 2(a)-2(b), 2(e)-2(f), and 3(a) of the main text are dominated by intra-bilayer terms of the form shown in Eq. (S10) for $\sigma \in \{A, B, C\}$. For the inter-bilayer terms, one may use Eq. (S11) with

$$K_h = Q'_h, \quad K_k = Q'_k, \quad K_l = \frac{1}{3}Q'_l \quad (\text{S16})$$

to see using Eq. (S4) that in the crystallographic basis

$$J_{AB}(\vec{Q}) \propto [\cos(\pi Q_h) + \cos(\pi Q_k)], \quad (\text{S17})$$

and hence that all modes are completely flat along $(1 \ 0 \ Q_l)$, as shown in Figs. 2(d) and 2(h) of the main text.

S5. MAGNETIC FORM FACTOR

The form factor describing magnetic scattering from ions with part-filled $3d$ and $4d$ electron shells, which are assumed to produce a spatially isotropic spin density, can be approximated in an intermediate $|\vec{Q}|$ range by [31]

$$F_{\text{iso}}(s) \approx \langle j_0(s) \rangle \approx \tilde{A}e^{-\tilde{a}s^2} + \tilde{B}e^{-\tilde{b}s^2} + \tilde{C}e^{-\tilde{c}s^2} + \tilde{D}, \quad (\text{S18})$$

where the variable s is defined as

$$s = \frac{\sin(\theta)}{\lambda} = \frac{|\vec{Q}|}{4\pi}. \quad (\text{S19})$$

The parameters $\{\tilde{A}, \tilde{a}, \tilde{B}, \tilde{b}, \tilde{C}, \tilde{c}, \tilde{D}\}$ are ion-specific and are tabulated in Ref. [31], where they are expressed without the tilde symbols (added here to avoid confusion with

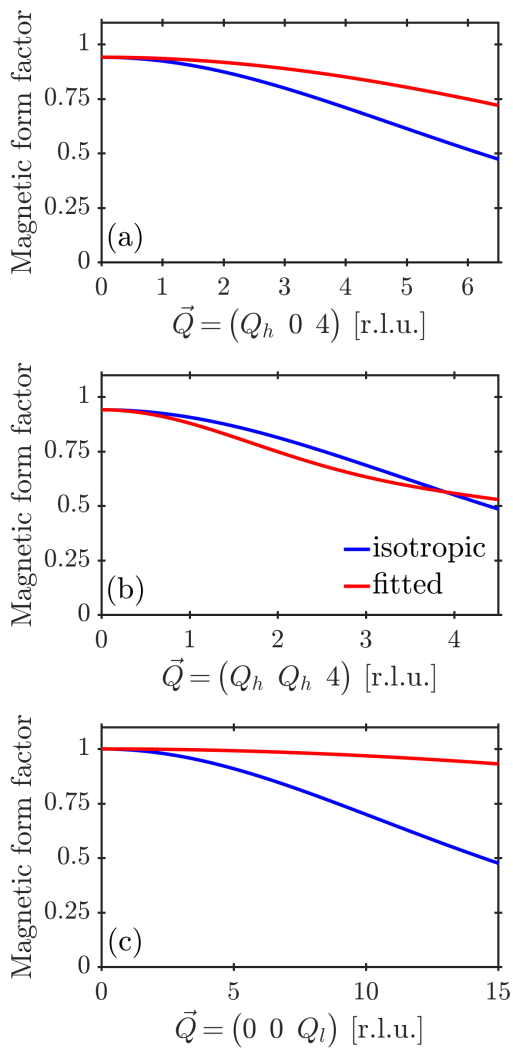


FIG. S3. Magnetic form factor shown for the high-symmetry \vec{Q} directions (a) $(Q_h 0 4)$, (b) $(Q_h Q_h 4)$, and (c) $(0 0 Q_l)$ in the crystallographic basis. Results for an isotropic spin density on the Cu^{2+} ions (solid blue lines) are compared with results obtained from optimal fits of the full scattered intensity in the measured data range (solid red lines), as described in the text. The magnetic form factor is normalized to 1 at $\vec{Q} = (0 0 0)$.

the bilayer labels and unit-cell parameters of our work).

The process of modelling the measured cross section for (coherent) inelastic magnetic scattering at low temperatures requires multiplying the magnetic dynamical structure factor by the square of the magnetic form factor. In our calculations of this cross section for the high-symmetry \vec{Q} directions measured in experiment, using the isotropic magnetic form factor for Cu^{2+} gives intensity functions that fall differently as functions of $|\vec{Q}|$ when compared to the data, as Fig. S3 makes clear. Thus we conclude from our results that the spin density of the Cu^{2+} ions in $\text{BaCuSi}_2\text{O}_6$ must indeed be anisotropic [18, 42]; this could be a consequence of hybridization ef-

fects that concentrate charge in the bilayer planes, analogous to those observed in the low-dimensional Cu^{2+} compounds La_2CuO_4 [32, 33] and SrCuO_2 [34, 35].

The consequence of this anisotropy is that the form factor falls more slowly with $|\vec{Q}|$ for the $(Q_h 0 4)$ and $(0 0 Q_l)$ directions than an isotropic function would dictate [Figs. S3(a) and S3(c)], whereas such behavior is not found along $(Q_h Q_h 4)$ [Fig. S3(b)]. To account for this effect, we have fitted our data using three separate functions with the form of Eq. (S18) for each of the directions $(Q_h 0 4)$, $(Q_h Q_h 4)$, and $(0 0 Q_l)$ while keeping fixed the value of the dynamical structure factor in our calculation.

S6. DIFFERENT SIGNS OF THE INTERACTION PARAMETERS

Changing the signs of the intra- and inter-bilayer interaction parameters has no effect on the density of triplon states. Thus the majority of experiments performed on $\text{BaCuSi}_2\text{O}_6$, including specific heat, magnetization, magnetic torque, magnetocalorimetry, and NMR, depend strongly on the magnitudes of these parameters but are very insensitive to their signs, which is one of the reasons why the sign of the intra-bilayer term has remained ambiguous for so long. Because the signs of these parameters were the crucial point of ambiguity in interpreting the earlier INS experiments, which we resolve in the present work, and because they are crucial to the frustration mechanism of dimensional reduction, in Fig. S4 we present calculations of the INS spectra that would be measured in $\text{BaCuSi}_2\text{O}_6$ under each possible scenario for AF or FM interactions. We consider only the physical modes of the minimal unit cell and show for reference the experimental spectra [Figs. 2(a)-2(d) of the main text].

Figures S4(e)-S4(f), S4(i)-S4(j), S4(m)-S4(n), and S4(q)-S4(r) illustrate the clear inversion of the in-plane mode dispersions caused by changing the intra-bilayer interactions from FM to AF. Specifically, the minima (the “bilayer gaps”) occurring in the crystallographic basis at even $(Q_h 0)$ and integer $(Q_h Q_h)$ for FM J' become maxima for AF J' , and conversely at odd $(Q_h 0)$ and half-integer $(Q_h Q_h)$.

Figures S4(g), S4(k), S4(o), and S4(s) illustrate the behavior of the two mode intensities in the almost non-dispersive $(0 0 Q_l)$ spectrum, where the double-peak structure is obtained for mode *A* when J'' is FM, whereas for AF J'' it appears for modes *B* and *C*; in each case the other modes have a single intensity peak. Figures S4(h), S4(l), S4(p), and S4(t) show that the completely non-dispersive mode energy along $(1 0 Q_l)$ is independent of the sign of J'' [Eq. (S11)], and in fact occurs in all circumstances when tetragonal symmetry of the inter-bilayer interactions is maintained. The same statement may be made for the effectively Q_l -invariant mode

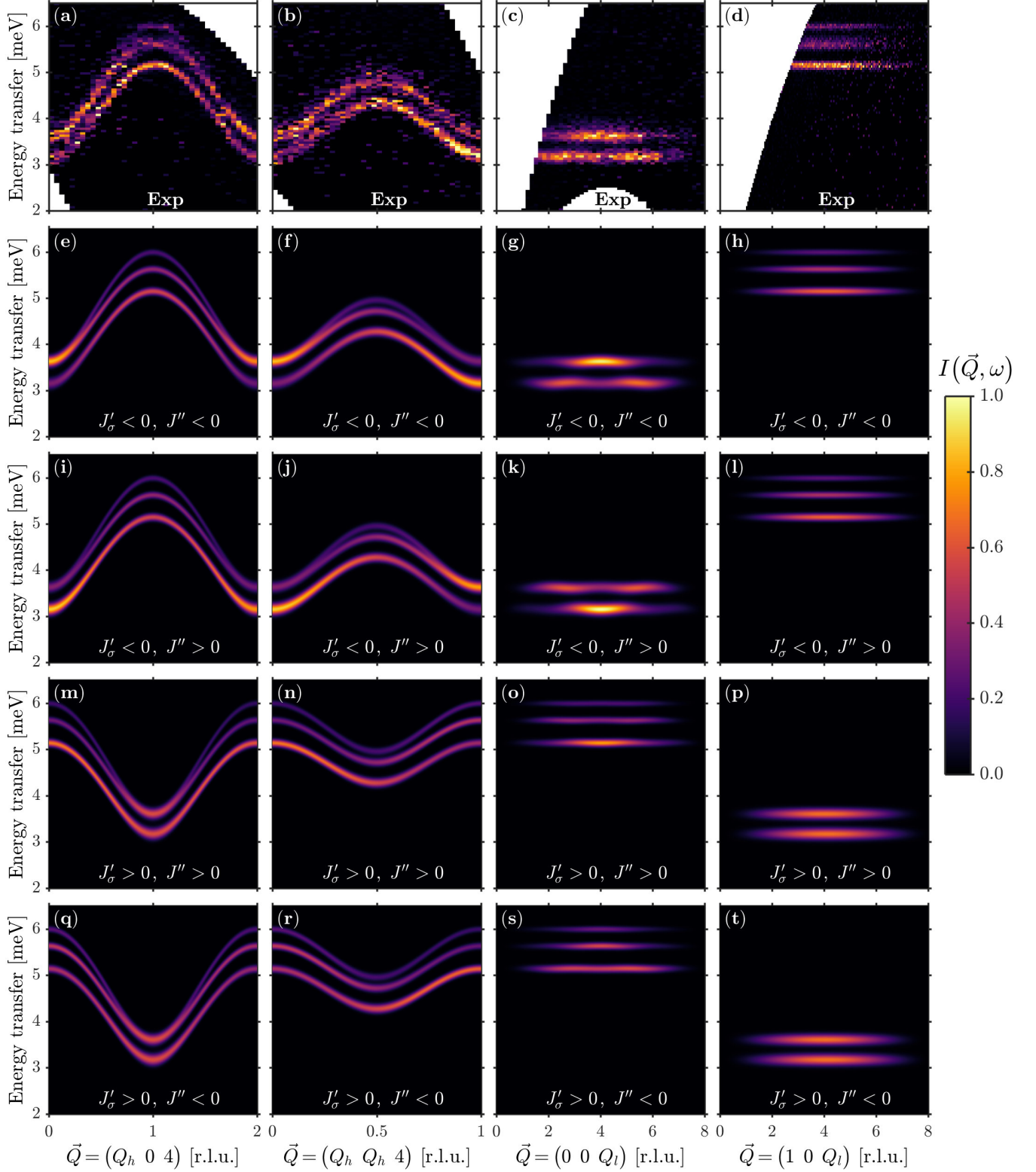


FIG. S4. (a)-(d) Experimental spectrum for four \vec{Q} directions, reproduced for reference from Fig. 2 of the main text. (e)-(t) Corresponding spectrum calculated by using the minimal model of Fig. 1(a) of the main text and with the magnitudes of the Heisenberg interaction parameters deduced for $\text{BaCuSi}_2\text{O}_6$, but taking different signs for the three intra-bilayer (J'_σ , $\sigma \in \{A, B, C\}$) and for the inter-bilayer (J'') interaction parameters. We show only cases where all three intra-bilayer interaction parameters have the same sign. (e)-(h) FM J'_σ and J'' , as in Figs. 2(e)-2(h) of the main text. (i)-(l) FM J'_σ and AF J'' . (m)-(p) AF J'_σ and J'' . (q)-(t) AF J'_σ and FM J'' .

intensity, which contains only the dimer form factor.

Before leaving this discussion, we comment briefly on the comparison between our optimal interaction parameters and those of previous neutron scattering studies. In the early work of Ref. [22], the data were fitted to a dimer model containing one dimer type and including only a next-nearest-neighbor intra-bilayer interaction, J'_2 , while the nearest-neighbor intra-bilayer term, our J'_σ , was set to zero. Although the intradimer interaction obtained by these authors, $J = 4.41(2)$ meV, is close to the average of the J_σ parameters we determine, the FM $J'_2 = -0.19(3)$ gives a dispersion far from the one we measure. With only these two parameters, the intra-bilayer spin structure consists of two disconnected but interpenetrating lattices and thus is not fully determined.

In the later work by some of the present authors [11], as noted in the main text and in Sec. S1, the analysis was affected by the sign ambiguity, caused by using the crystallographic unit cell, and by the historical assumption of AF intra-bilayer interactions. The intradimer and intra-bilayer interaction parameters of this study are close in magnitude to our present results, but with larger error bars. In addition to refining the accuracy and signs of these terms, here we obtain entirely new information in the size and sign of the inter-bilayer interaction, J'' . Because the size of J'' we deduce exceeds the upper limit thought to be consistent with the results of Ref. [11], our minimal model does not require any modulation of the inter-bilayer interaction, of the type proposed in Ref. [8], to explain any of the available BaCuSi₂O₆ data. We stress again that the sign of J'' is not the crucial ingredient delivering inter-bilayer frustration, as this is present for either sign of J'' if the J'_σ parameters are AF, but for neither when they are FM.

S7. RELATIVE FRACTIONS OF BILAYER TYPES

For a more general expression of the case $(1\ 0\ Q_l)$ of the previous subsection, in any structurally dimerized material with more than one dimer type, one may define \vec{Q}^* as the subset of \vec{Q} space where the Fourier transform of the interactions between dimers on different sublattices is identically zero. For \vec{Q} points in \vec{Q}^* , the dimer sublattices are effectively decoupled and one may approximate the inelastic magnetic cross section, using the dynamical structure factor for each separate dimer sublattice [Eq. (S12)], by

$$\left. \frac{d^2\sigma}{d\Omega d\omega}(\vec{Q}, \omega) \right|_{\vec{Q} \in \vec{Q}^*} = \mathcal{N}(\vec{Q}, \omega) \sum_{\rho} \frac{N_{\rho} J_{\rho}}{\omega_{\rho}(\vec{Q})} \delta(\omega - \omega_{\rho}(\vec{Q})), \quad (\text{S20})$$

where all terms independent of the dimer sublattice, including the Debye-Waller factor, the magnetic form factor, and k_f/k_i , are contained in the prefactor $\mathcal{N}(\vec{Q}, \omega)$.

N_A^{rel} [%]	N_B^{rel} [%]	N_C^{rel} [%]
51(5)	32(4)	17(2)

TABLE S1. Relative intensities of excitations corresponding to bilayer types A , B , and C .

Convolving the δ functions with the instrumental resolution function of the spectrometer yields finite-width line shapes that are usually approximated as Gaussians.

BaCuSi₂O₆ presents an especially straightforward case where the separate dimer sublattices (ρ) are the A , B , and C bilayers. From Eqs. (S11) and (S4) one may read that \vec{Q}^* includes all points with $Q'_h = Q'_k = Q'_l/3 = \pm(2n+1)/2$, where n is an integer. More specifically, from Eq. (S17) it is clear that $(1\ 0\ Q_l)$ is contained within \vec{Q}^* for all Q_l . $(1\ 0\ Q_l)$ has the additional advantage that the A , B , and C modes are maximally separated in energy (Fig. 2 of the main text). Because the triplon modes along $(1\ 0\ Q_l)$ are completely flat, the statistical accuracy can be increased by integrating over a very wide range in Q_l . Using our data from AMATERAS, we extracted the function $I^*(\omega)$ by integrating over $[0.95, 1.05]$ in Q_h , $[-0.05, 0.05]$ in Q_k , and $[4, 8]$ in Q_l ; in the inset of Fig. 2(h) of the main text, we chose to label the Q_l coordinate by \bar{Q}_l to reflect this extraordinarily wide integration window. As this inset makes clear, $I^*(\omega)$ displays three narrow and well-separated peaks, which we fit using three Gaussians (plus a background term). By integrating each Gaussian over its full energy, we obtain one intensity parameter, I_{ρ} , for each bilayer.

By using Eq. (S20) we then determine the relative fractions of the three different dimer types using

$$N_{\rho}^{\text{rel}} = \frac{N_{\rho}}{\sum_{\eta} N_{\eta}} = \frac{I_{\rho} \omega_{\rho} / J_{\rho}}{\sum_{\eta} I_{\eta} \omega_{\eta} / J_{\eta}}, \quad (\text{S21})$$

where the sublattice energy scale, J_{ρ} , is the intradimer interaction and ω_{ρ} is the energy of each non-dispersive band in Figs. 2(d) and 2(h) of the main text. The results for N_{ρ}^{rel} are displayed in Table S1 and verify at the 5% accuracy level that the bilayer ratio is indeed 3:2:1. We stress that this analysis is completely independent of the bilayer stacking order and the actual value of the inter-bilayer interaction parameter, J'' .

S8. QUANTUM MONTE CARLO

We have performed large-scale QMC simulations using the stochastic series expansion (SSE) algorithm [46] on 3D cubic lattices of sizes $L \times L \times L_{\perp}$, with $L_{\perp} = 3L$, for $L = 8, 10, 12, \dots, 22$. The critical temperature, T_c , is extracted for each applied field, H , by using the finite-size analysis of the superfluid density, ρ_{sf} , of the hard-core bosons representing the triplons. In the magnetic

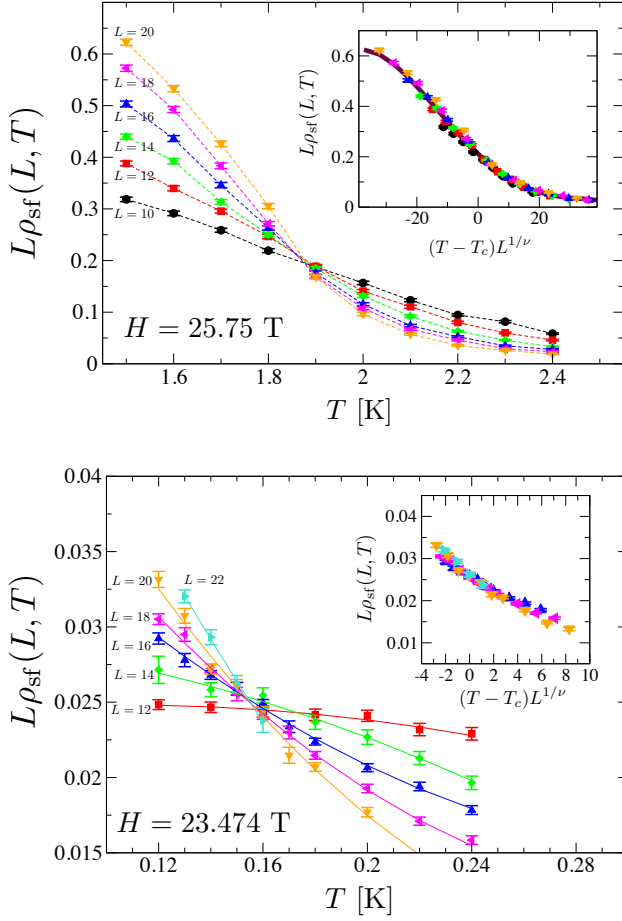


FIG. S5. Scaled spin stiffness, $L\rho_{\text{sf}}(L, T)$, shown for all values of L in our simulations to illustrate the unique crossing point for two values of the magnetic field. The extracted value of T_c allows the scaling collapse shown in the insets. As H approaches H_{c1} (lower panel), ρ_{sf} becomes very small and a large relative error becomes inevitable.

context, the superfluid density is equivalent to a spin

stiffness. Because $L^{d+z-2}\rho_{\text{sf}}(L, T)$ has scaling dimension zero, $d = 3$ here and $z = 0$ for a finite-temperature transition, all curves $L\rho_{\text{sf}}(L, T)$ for different L cross at the same point, $T = T_c$ [48], as illustrated for two values of H in Fig. S5. With T_c fixed in this way, one may extend similar arguments to discuss the thermal scaling, which is governed by the finite-size form [48]

$$\rho_{\text{sf}}(L, T) = L^{2-d}\mathcal{F}[L^{1/\nu}(T - T_c)]. \quad (\text{S22})$$

As the insets of Fig. S5 make clear, good data collapse is achieved using a value $\nu = 0.66$ for the critical exponent of the correlation length, in excellent agreement with the best available estimate for this universality class (3D XY) of $\nu = 0.672$ [36].

As shown in Fig. 4(a) of the main text, our QMC simulations provide an excellent quantitative account of the entire (H, T) phase boundary of $\text{BaCuSi}_2\text{O}_6$. In the challenging regime near the field-induced QPT at H_{c1} , the physics of the system is determined by the mobility of the triplets condensing in the A bilayers at fields where the B and C bilayers, whose associated dispersion gaps have not yet closed (Fig. 2 of the main text), contain only low, “proximity-induced” triplet densities (Fig. 4(b) of the main text). From Eq. (1) of the main text, perfectly frustrated inter-bilayer coupling [14] would in fact allow $t_c^{\text{eff}} = 0$, no field-linear component in ρ_B or ρ_C , and possible $\phi = 1$ scaling over some range of h_{window} . Nevertheless, the true QPT is always a 3D phenomenon, because at $T = 0$ K the system does develop spatial coherence in all three dimensions on some low energy scale.

Away from perfect frustration, and in particular for $\text{BaCuSi}_2\text{O}_6$, $t_c^{\text{eff}} \neq 0$ ensures both 3D and anomalous (h_{window} -dependent) scaling over regimes of finite width. We comment that the windowing procedure is extremely sensitive to the chosen value of H_{c1} ; this is not an issue in our present calculations, because H_{c1} is fixed by the interactions determined from INS, but when H_{c1} is also an unknown to be fitted simultaneously [3], changes of 0.01 T can cause changes of order 0.1 in ϕ .